

NASA Technical Memorandum 87186

NDE of Structural Ceramics

(NASA-TM-87186) NDE OF STRUCTURAL CERAMICS
(NASA) 14 P HC AC2/HF A01 CSCL 14D

N86-16598

G3/38 Unclass
05209

Stanley J. Klima and Alex Vary
Lewis Research Center
Cleveland, Ohio



Prepared for the
31st International Gas Turbine Conference
sponsored by the American Society of Mechanical Engineers
Dusseldorf, West Germany, June 8-12, 1986



NDE OF STRUCTURAL CERAMICS

Stanley J. Klima and Alex Vary
National Aeronautics and Space Administration
Lewis Research Center
Cleveland, Ohio 44135

ABSTRACT

Radiographic, ultrasonic, scanning laser acoustic microscopy (SLAM), and thermo-acoustic microscopy techniques were used to characterize silicon nitride and silicon carbide modulus-of-rupture test specimens in various stages of fabrication. Conventional and micro-focus x-ray techniques were found capable of detecting minute high density inclusions in as-received powders, green compacts, and fully densified specimens. Significant density gradients in sintered bars were observed by radiography, ultrasonic velocity, and SLAM. Ultrasonic attenuation was found sensitive to microstructural variations due to grain and void morphology and distribution. SLAM was also capable of detecting voids, inclusions, and cracks in finished test bars. Consideration is given to the potential for applying thermo-acoustic microscopy techniques to green and densified ceramics. The detection probability statistics and some limitations of radiography and SLAM also are discussed.

INTRODUCTION

Concern over exhaust gas emissions and a need for higher fuel efficiency and adaptability to alternate fuels has created a keen interest in ceramics for advanced automotive heat engine applications. Potential efficiency improvements as high as 30 to 50 percent over current engine technology have been estimated for engines with major ceramic components (1). The energy saving potential arises from higher permissible operating temperatures and reduced friction, weight, and inertia stemming from the mechanical and physical properties of ceramics.

Although leading candidate materials based on silicon carbide and silicon nitride have good average high temperature strength and excellent oxidation resistance, they also exhibit variability in mechanical properties and relatively low fracture toughness (1-3). Variation in mechanical properties is generally attributed to discrete defects such as cracks, voids, and inclusions introduced during processing (4-6). Improvements in component reliability can be achieved by screening out defective parts through nondestructive

inspection before putting them into service. Current cost effective fabrication procedures also frequently produce ceramics with bulk density variations and microstructural anomalies that escape detection by conventional methods but can still degrade performance and reliability (7). Therefore, it is essential to have nondestructive evaluation (NDE) techniques capable of producing measurements that indicate when the desired microstructures and elastic properties have been achieved.

There also exists the possibility of reducing the cost of fabrication by utilizing NDE techniques in the early stages of processing to avoid the expense of finishing parts from flawed material. Even more importantly perhaps, if NDE techniques were incorporated into a ceramic materials technology development program, information might be obtained regarding the source of defects and steps could be taken to minimize their occurrence through improved fabrication methods. Thus, NDE has the potential for reducing the effort expended in a materials research program and shortening the time needed to develop strong, reliable structural ceramics.

This paper describes investigations conducted at the Lewis Research Center and discusses findings on the applicability of radiographic, ultrasonic, scanning laser acoustic microscopy (SLAM), and thermo-acoustic techniques for characterizing silicon nitride and silicon carbide materials in various stages of fabrication. Pertinent results are presented along with cursory descriptions of the NDE processes. Emphasis is placed on the development of flaw detection reliability statistics for radiography and SLAM.

RADIOGRAPHY

X-ray methods can be used to evaluate ceramic materials in all stages of specimen fabrication. Figure 1 contains radiographs of four pairs of modulus-of-rupture (MOR) bars, each sintered under a different set of conditions. The radiographs exhibit significant density variations. The variations are caused by differences in x-ray absorption, which is directly proportional to the number of atoms encountered by the x-ray beam passing through the material. Thus, the darkest

regions on the radiographic prints represent zones of highest material density while the lighter shades of gray indicate zones having proportionally lower density. It is evident from the bulk density measurements as well as from the radiographs that densification was affected by both time at temperature and the way in which the specimens were separated from each other during firing. For example, after 1 hr at 2140 °C, the specimens separated by boron nitride disks (minimum contact area) had a bulk density 4 percent higher than the specimens separated by a thin layer of BN powder. The difference appears to be primarily in the size of the low density zone in the core of the specimens as evidenced by radiographs of the two specimen pairs. On the other hand, the specimens sintered for 1 hr in minimum contact with disk spacers had the same bulk density as specimens sintered for 4 hr in full contact with disk spacers. The radiographs show, however, that the former exhibit a low density core while the latter appear to have relatively uniform density distribution over the entire specimen. Specimens sintered for only 2 hr in full contact with BN disks also had a relatively uniform density distribution but only slightly lower bulk density. Thus, it is evident that radiography can provide details on material densification during the sintering process that cannot be obtained as readily in any other way. It should be noted that the information presented here is intended only to illustrate the manner in which radiography can be used to advantage to speed the development of improved fabrication/processing techniques. Final conclusions regarding optimized sintering conditions for silicon nitride await the results of further studies.

The x-ray technique was also used to detect foreign particles, particularly those with relatively high density compared to silicon nitride and silicon carbide. The x-ray absorption coefficient varies directly as a function of atomic number, therefore the greater the difference between the foreign particle and the matrix material the greater the film contrast on the radiograph, and generally the smaller the particle that can be imaged. Figure 2 presents radiographs of a single MOR bar taken after three stages of processing. All three radiographs contain tiny dark spots which represent the location of high density inclusions. Particular attention should be given to two prominent inclusions just to the right of center of the specimen. These particles persisted throughout the fabrication cycle with little or no modification during firing and were sufficiently deep that they were not removed by surface grinding of the test bar. The specimen contains a greater number of high density particles in the green state than in the as-fired condition. This suggests that many of green state inclusions may consist of agglomerations of certain oxides that were added to aid the densification process. During sintering, the oxides (e.g., Y_2O_3 and SiO_2) contribute to the formation of a glassy phase which becomes diffuse and can not be detected by x-rays. Some defects also disappear after surface grinding. For example, the number 2 was inscribed in the surface of the green specimen after pressing to identify it as being from batch two. The number shows up as a white object because the inscription is essentially a curvilinear void. The number is also seen in the radiograph made after firing but note that both the number and the specimen dimensions have shrunk significantly due to material densification. After surface grinding of course, the batch number no longer exists in either the radiograph or the specimen.

Some inclusions found in green compacts were analyzed after removing the outer layers of specimen material to bring the particles to the surface. The

compositions of typical heavy density inclusions are listed in the table of Fig. 2. Iron was most frequently encountered while other materials such as tin and nickel base alloy particles were uncommon. One particle was identified as Ce rich, indicating that it may be an agglomerate composed of Ce_2O_3 , which was used as a sintering aid in that specimen. Although it is suspected from radiographic evidence that many such oxide agglomerates exist, they are very difficult to locate for analysis because their physical appearance is very much like the matrix and therefore difficult to identify visually. The particle sizes listed in the table are typical of the few particles that were analyzed and do not necessarily represent the smallest detectable size.

Samples of as-received powder were also radiographed to determine if any foreign particles were present prior to in-house processing. Figure 3 shows radiographs of lightly compacted disks which contain numerous high density particles indicating that, other than the oxide additives, most high density inclusions originated during production of the starting powders. Clearly, methods of producing ceramic starting powders must be improved or some method for removing foreign particles must be devised to clean up the powder before making green compacts.

SCANNING LASER ACOUSTIC MICROSCOPY

The scanning laser acoustic microscope (SLAM) was used for detection of surface and near surface defects as well as for revealing patterns of density variations. Figure 4 contains two amplitude mode acoustic micrographs showing three types of defects in silicon nitride. Flaw A is a surface connected inclusion about 75 μm diameter. The same inclusion was detected by x-rays as a high density particle and, since it was surface connected, it could also be seen optically at magnifications of $\times 10$ to $\times 30$. Flaw B is a planar crack-like defect which is also surface connected and could be seen optically. However, it was not detected by x-rays because it is essentially two-dimensional and not oriented exactly parallel to the x-ray beam, and therefore not resolved on the radiograph. Flaw C is also a crack-like feature but is situated beneath the surface. Although it was easily detected by the SLAM, it could not be resolved by either radiographic or optical methods. In addition to the discrete defects just described, the SLAM images also exhibit a background consisting of long straight linear indications caused by diamond grinding grooves, and small ripples not associated with any obvious feature. It is probable that the tiny ripples are caused by microstructural features which diffract the general sound field but are too small and too numerous to be resolved individually. More work is required to determine the nature of these very small scattering sites and what effect they may have on ceramic material properties.

Scanning laser acoustic microscopy can also be used in the interference mode (8) to obtain information regarding bulk density variations. In a specimen with constant thickness, the time of travel of an ultrasonic wave provides a measure of sound velocity, and velocity can be used to infer material density (9). SLAM interferograms can be used to image velocity variations that occur within the viewing field as shown in Fig. 5. Any deviation in time of travel will cause the interference fringes to bend to the right or left. The relatively straight fringes in Fig. 5(a) imply that, within the field of view (2.75 by 2.0 mm), the density of the ceramic specimen is relatively uniform. In Fig. 5(b) however, the density at the bottom (near the edge of the MOR bar) is significantly greater than at the top

of the image which is located a little over 2 mm away from the specimen edge.

ULTRASONIC VELOCITY AND ATTENUATION

Ultrasonic velocity and attenuation measurements were used to characterize density and microstructure in monolithic silicon nitride and silicon carbide. Research samples exhibiting a wide range of density and microstructural variations were used to demonstrate that bulk density variations correlate with and can be estimated by velocity measurements (Fig. 6). Variations in microstructure (grain size and shape or void size and distribution) in silicon carbide had only a slight effect on velocity (9). Although significant variations in certain microstructural features had only a slight effect on ultrasonic velocity it was observed that the same variations had a profound effect on attenuation of high frequency ultrasonic waves. Figure 7 shows a plot of attenuation as a function of ultrasonic frequency for some of the same specimens used in the velocity-density study. Eight silicon carbide samples, all with similar bulk densities were selected. The specimens were divided equally into sets with two widely differing microstructures as shown in Fig. 7. The plot shows that attenuation in the large grained material is at least four times higher than for the small grained material. Although the grain size is the most obvious microstructural difference between the two sample groups, there also exist other features that could affect ultrasonic attenuation as well as material properties. For example, the less attenuating material has equiaxed grains while many grains in the more attenuating material are elongated or rod-like in shape. The void size and morphology is also quite different. Although the total porosity is the same for the two sample groups as evidenced by the measured bulk density, the photomicrographs show that voids are larger but fewer in number in the more attenuating material. It is probable that all of the variations in microstructure just described have a cumulative effect on total measured attenuation in the ceramic samples. It is not clear which feature has the greatest effect at this time because the variables cannot be readily separated during thermomechanical processing of the materials.

Modulus of rupture test results from the samples show that the material with the fine microstructure is significantly stronger at room temperature than the coarser material. This suggests that ultrasonic attenuation measurements may be useful as a quality control tool to assure material strength to the extent that is controlled by microstructure. It should be noted however, that such a relationship may be valid only as long as composition is unchanged. For example, the authors of Ref. 10 reported MOR results for silicon nitride with four different rare-earth additives. The composition that yielded the highest strength also exhibited the largest grain size. Obviously more work is needed in this area.

THERMO-ACOUSTIC IMAGING

Like the x-ray technique, thermo-acoustic imaging can be used in a noncontacting, noninvasive mode. Commonly referred to as photoacoustic microscopy, photoacoustic spectroscopy, or thermal wave imaging (11-14), the technique essentially measures relative differences in surface and near-surface thermal properties of the material being evaluated. The absorption of intensity modulated electromagnetic radiation focused at any point on the sample gives rise to localized cyclic heating and cooling which generates

elastic waves. The amplitude and phase of these waves can be measured at another point on the specimen surface with a piezoelectric crystal or in the surrounding medium by a sensitive microphone. Thermo-acoustic waves may be generated by absorption of laser light or an electron beam, but other forms of electromagnetic energy such as microwaves, infrared, or x-rays might also be used. Laser methods are also being considered for receiving these signals (14). This would add to the versatility and flexibility of the thermo-acoustic technique.

A schematic diagram of a system utilizing a scanning electron beam heating source and a piezo-electric acoustic sensor contained in a scanning electron microscope envelope is shown in Fig. 8. Figure 9 contains a SEM backscatter image alongside a thermo-acoustic image of the same region near the edge of a silicon carbide specimen. The SEM image shows a portion of a crack that originates at the edge, as well as dust particles on the specimen surface. The thermo-acoustic image clearly shows the subsurface extension of the crack in addition to the optically visible portion. Note, however, that the surface dust was not registered by the thermo-acoustic interrogation. Thus, the thermo-acoustic technique shows promise for detection of surface and near-surface discontinuities in ceramics.

FRACTURE MECHANICS AND NDE RELIABILITY

The reliability of an NDE procedure is defined as the efficiency of that procedure in detecting flaws of a specific type and size. After nondestructive examination it cannot be said that a particular component is entirely free of flaws simply because none were found; it can only be asserted that there is a certain probability that the part is free of defects of a specific type and size (15). The higher the level of this probability, the higher the reliability of the NDE procedure and therefore the higher the reliability of the part that was inspected.

The need for quantitatively assessing the reliability of flaw detection has arisen from the application of fracture mechanics principles to the design of critical parts. The fracture mechanics concept assumes the existence of flaws and quantitatively describes their effect on strength. Thus, a critical crack size is defined for a particular material and loading condition. The role of NDE is to assure that flaws corresponding to the critical crack size for fracture at the design load are absent when the part is put into service. Furthermore, it may be necessary to guarantee that flaws much smaller than the critical size are absent to account for possible subcritical crack growth, especially where stress corrosion or fatigue cracking may be encountered.

The use of fracture mechanics concepts places a premium on the ability of nondestructive inspection to detect small defects, and on the need to determine the practical reliability of a particular NDE procedure when that procedure is used to detect flaws of a specific type and size. If the design is such that the critical crack size is greater than the smallest flaw that can be reliably detected by a particular technique, then that technique can be used. The difference between the critical size and the smallest detectable size is a measure of the factor of safety (albeit not the conventional definition of safety factor).

An example of NDE reliability data generated for SLAM and radiographic techniques, according to the guidelines set forth in Ref. 15, is presented in Figs. 10 and 11 in the form of plots of probability of detection as a function of void size. The curves

define the lower limit of probability of detection (a conservative estimate) calculated at a confidence level of 95 percent using the binomial distribution. Details are given in Refs. 16 and 17. The significance of reliability data is that it provides information regarding the size of flaws that can be detected with a reasonable degree of reliability. For example, Fig. 10(b) shows that the probability of detection is 90 percent or higher for void diameters equal to or greater than 1.5 percent of specimen thickness when using the microfocus x-ray technique. For conventional radiography similar probabilities of detection are indicated only for voids exceeding 2.5 percent of specimen thickness. The plots also show that smaller voids can sometimes be detected, but with lower detection reliability. For SLAM technique, the plot (Fig. 11) shows that detectability is significantly improved by polishing the specimen surface. Thus, the designer must take into consideration the surface finish of a component in order to assure that it is inspectable. The designer can utilize this type of data to determine the largest flaw that will be missed a significant proportion of time, and take steps to ensure that operating stresses are adequate to prevent that size flaw from becoming critical. Very little data of this type exists today, particularly for structural ceramics. All too often, the smallest detectable flaw sizes are reported for specific techniques with no regard to the probabilistic nature of the NDE process.

CONCLUDING REMARKS

Investigations conducted at NASA Lewis showed that radiography is a versatile tool for NDE of ceramics. Because the method is nonconnecting and noninvasive, x-rays can be used at all stages of fabrication to detect density gradients, and volumetric flaws such as high density inclusions, oxide agglomerates, and discrete voids. The probability of detection of voids was higher for microfocus x-ray techniques than for conventional methods but the conventional methods were faster. Radiographic sensitivity to volumetric flaws is excellent whenever the x-ray absorption coefficient of the flaw differs significantly from the matrix material as is the case for high density inclusions. Unfortunately, this is not true for loose agglomerations of matrix powder particles. The sensitivity to cracks is also poor unless the plane of the crack is almost exactly aligned with the direction of the x-ray beam and the crack is not tight (tight cracks have essentially no volume).

Scanning laser acoustic microscopy was found useful for detecting surface and near surface defects in densified ceramics. Unlike radiography, the technique is capable of detecting both volumetric and crack-like flaws. The sensitivity to tight cracks is good except when the plane of the crack is aligned parallel to the ultrasonic beam. (The orientation that is worst for radiography is best for ultrasonics). Surface finish is important for flaw detection since as-fired surfaces present a much higher background noise level than diamond ground or polished surfaces. The probability of detection is significantly different for each condition. Ceramics with a high level of porosity (densities less than 80 percent of theoretical) also present a problem because the large number of pores scatter the sound waves. In the interference mode, the SLAM can also provide a qualitative indication of density variations by virtue of the effect on ultrasonic velocity.

Ultrasonic velocity and attenuation measurements were determined to be useful for characterizing ceramics in terms of density and microstructure. Bulk densities of silicon nitride and silicon carbide correlate with and can be estimated by velocity measurements. Although variations in certain microstructural features had only a minor effect on velocity they had a strong effect on ultrasonic attenuation. It appears that attenuation measurements may be useful for ranking ceramic specimens or components, of a given composition, according to relative strength.

There is a need for quantitatively assessing the reliability of flaw detection for each NDE technique and material combination if fracture mechanics principles are to be effectively utilized in design of ceramic engine components. With this information the designer can determine the largest size flaw that will be missed a significant proportion of time, and take steps to ensure that operating stresses are adequate to prevent that size defect from becoming critical.

REFERENCES

1. Johnson, D.R., et al: Ceramic Technology for Advanced Heat Engines Project. Am. Ceram. Soc. Bull., vol. 64, no. 2, Feb. 1985, pp. 276-281.
2. Richerson, D.W.: Evolution in the U.S. of Ceramic Technology for Turbine Engines. Am. Ceram. Soc. Bull., vol. 64, no. 2, Feb. 1985, pp. 282-286.
3. Bubsey, R.T.; Shannon, J.L.; and Munz, D.: Development of Plane Strain Fracture Toughness Test for Ceramics Using Chevron Notched Specimens. Ceramics for High-Performance Applications III: Reliability. E.M. Leno, R.N. Katz, and J.J. Burke, eds., Plenum Press, 1985, pp. 753-771.
4. Bowen, H.K., et al: Basic Research Needs on High Temperature Ceramics for Energy Applications. Mater. Sci. Eng. vol. 44, 1980, pp. 1-56.
5. Rice, R.W., et al: Failure Causing Defects in Ceramics; What NDE Should Find. NRL-MR-4075, Naval Research Laboratory, Oct. 1979. (AD-A078234.)
6. Baumgartner, H.R.; Brockelman, R.H.; and Hanson, P.M.: Development of Nondestructive Testing Techniques for High Performance Ceramics. AMMRC TR-78-11, Army Materials and Mechanics Research Center, Jan. 1978. (AD-A059063.)
7. Lange, F.F.: Fracture Mechanics and Microstructural Design. Fracture Mechanics of Ceramics, vol. 4, R.C. Bradt, D.P.H. Hasselman, and F.F. Lange, eds., Plenum Press, 1978, pp. 799-819.
8. Kessler, L.W., Yuhas, D.E. and Vorres, C.L.: Acoustic Microscopy of Ceramics. Proceedings of the DARPA/AFWAL Review of Progress in Quantitative NDE, AFWAL TR-81-4080, Sept. 1981, pp. 128-135. (AD-A108741.)
9. Klima, S.J., et al: Ultrasonic Velocity for Estimating Density of Structural Ceramics. NASA TM-82765, 1981.
10. Sanders, W.A. and Mieskowski, D.M.: Strength and Microstructure of Sintered Si_3N_4 With Rare-Earth-Oxide Additions. Am. Ceram. Soc. Bull., vol. 64, no. 2, Feb. 1985, pp. 304-309.
11. Rosenzweig, A., and Gersho, A.: Theory of the Photoacoustic Effect with Solids. J. Appl. Phys., vol. 47, no. 1, Jan. 1976, pp. 64-69.
12. Wong, Y.H., Thomas, R.L., and Hawkins, G.F.: Surface and Subsurface Structure of Solids by Laser Photoacoustic Spectroscopy. Appl. Phys. Lett., vol. 32, no. 9, May 1, 1978, pp. 538-539.

13. Rosencwaig, A.: Photoacoustic Microscopy. Am. Lab., vol. 11, no. 4, Apr. 1979, pp. 39-40, 42, 47-49.
14. Thomas, R.L., et al: Scanning Photoacoustic Microscopy of Aluminum with Aluminum Oxide, Roughness Standards and Rubber. U.S. Army Tank-Automotive Command, TACOM TR-12957, June 1984. (AD-A149460.)
15. Packman, P.F., Klima, S.J., Davies, R.L., Malpani, J., Moyzis, J., Walker, W., Yee, B.G.W., and Johnson, D.P.: Reliability of Flaw Detection by Nondestructive Inspection. Metals Handbook, vol. 11, American Society for Metals, 1976, pp. 414-424.
16. Baakloui, G.Y.; Kiser, J.D.; and Roth, D.J.: Radiographic Detectability Limits for Seeded Voids in Sintered Silicon Carbide and Silicon Nitride. NASA TM-86945, 1984.
17. Roth, D.J., et al.: Reliability of Void Detection in Structural Ceramics Using Scanning Laser Acoustic Microscopy. NASA TM-87035, 1984.

ORIGINAL PAGE IS
OF POOR QUALITY


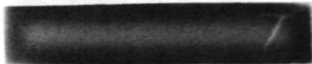




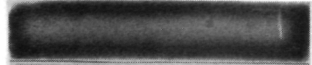

THRU-THICKNESS RADIOGRAPH	SINTERING TIME AT 2140 °C	SPECIMEN SPACERS	MEAN BULK DENSITY, G/CC
	1 HR	BN DISK MIN CONTACT	3.17
			3.18
	4 HR	BN DISK FULL CONTACT	3.17
			3.17
	2 HR	BN DISK FULL CONTACT	3.16
			3.14
	1 HR	BN POWDER FULL CONTACT	3.03
			3.06

Figure 1. - Illustration of the use of X-rays to monitor densification of silicon nitride MOR bars sintered under various conditions. Radio-graphs show how different combinations of time-at-temperature and specimen spacer arrangement can alter material density distribution.

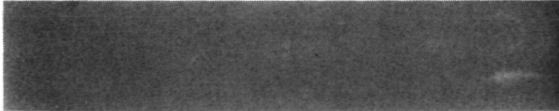
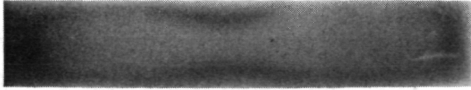
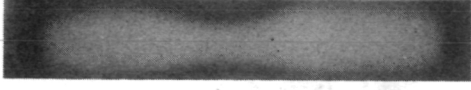
		
GREEN COMPACT (ISOPRESSED)		
	REPRESENTATIVE INCLUSIONS DETECTED AND ANALYSED	
AS-FIRED MOR BAR	TYPE	SIZE, % THICKNESS
	Fe	0.5
MOR BAR AFTER GRINDING	Sn	0.5
	Ni, Cr, Co, Ti	1.3
	Ce rich	1.5

Figure 2. - Illustration of the use of radiography to detect and monitor high density foreign particles throughout the fabrication process. Chemical analysis was performed on selected samples taken from the green silicon nitride compacts.

ORIGINAL PAGE IS
OF POOR QUALITY

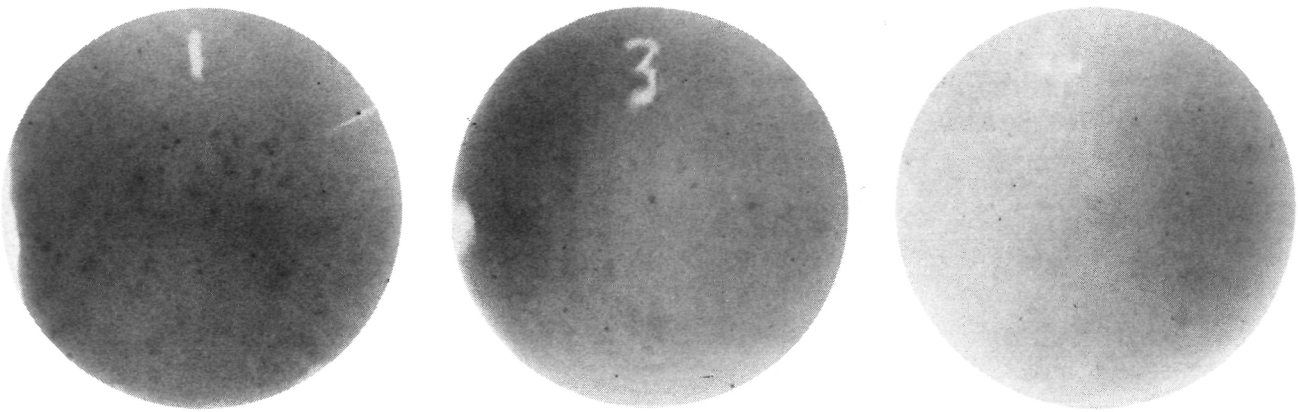


Figure 3. - Radiographs of as-received Si₃N₄ powder showing high density inclusions (dark specks). Disks were made by lightly compacting dry powder in a die at 56 MPa to a final thickness of 3 mm.

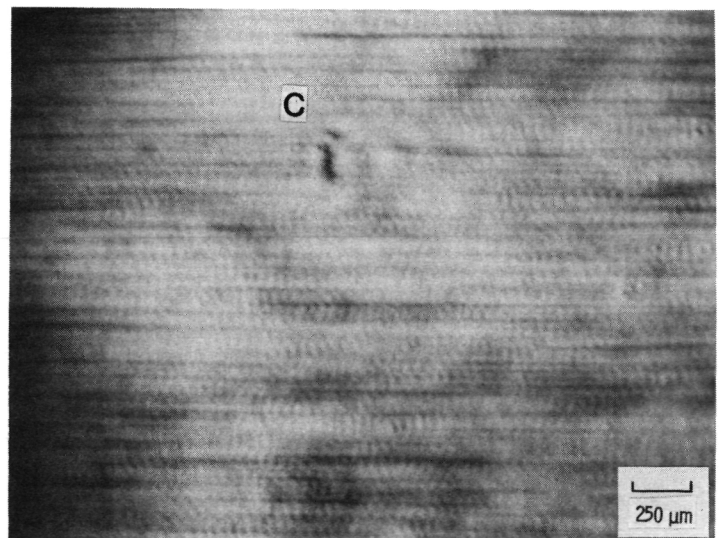
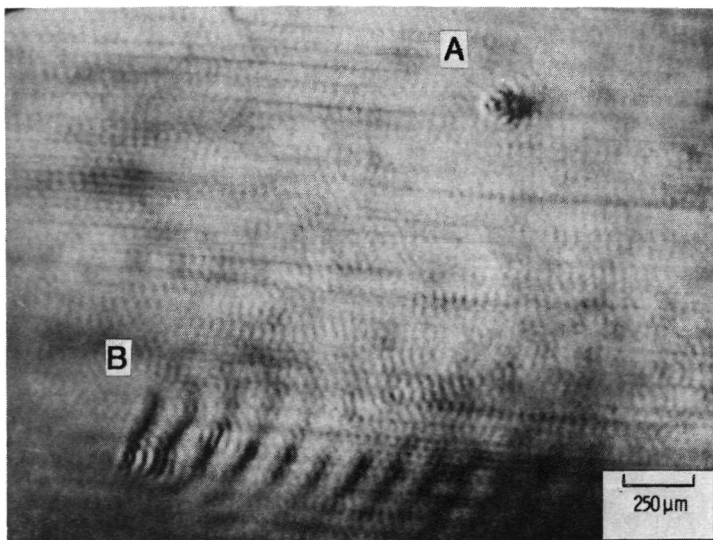
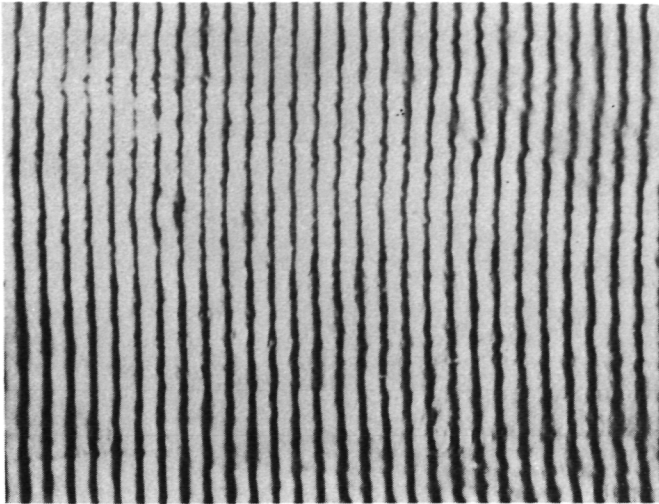
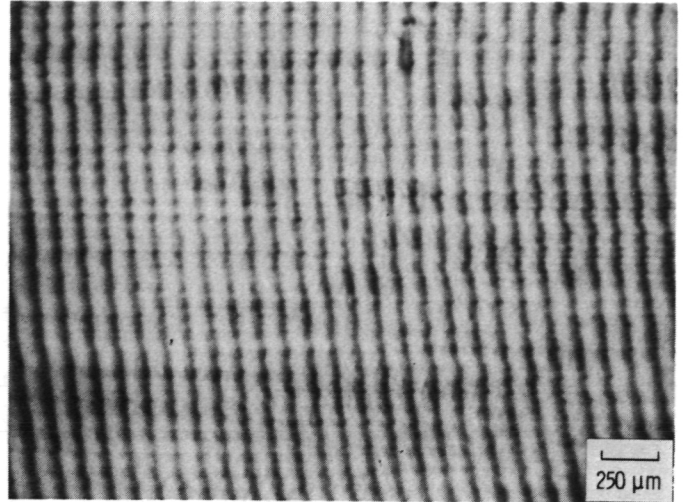


Figure 4. - SLAM micrographs illustrating images of two surface-connected flaws (A and B) and near-surface flaw (c) in diamond-ground silicon nitride specimen.

ORIGINAL PAGE IS
OF POOR QUALITY



(a) Density is essentially uniform.



(b) Density increases top to bottom.

Figure 5. - Interferograms produced by the scanning laser acoustic microscope illustrating a capability for imaging density gradients in Si_3N_4 MOR bars.

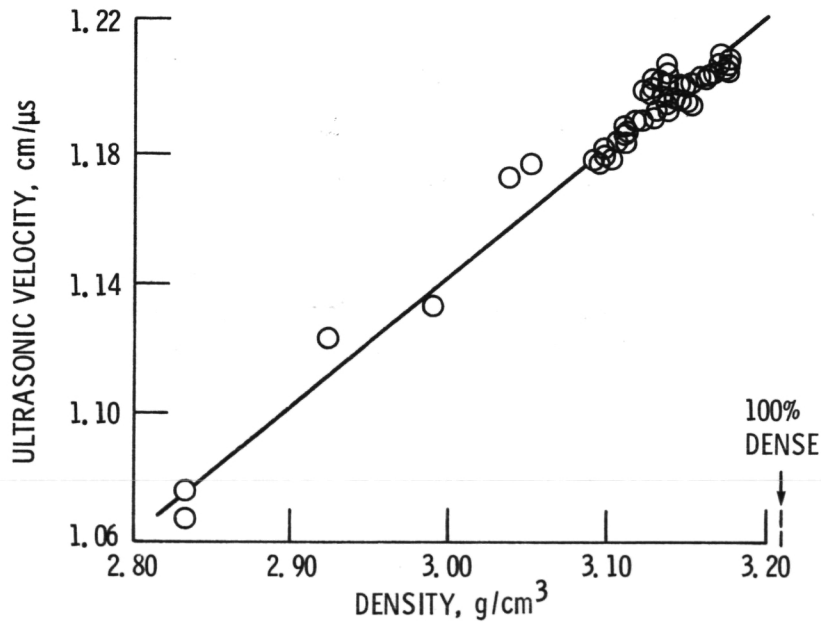


Figure 6. - Relationship between ultrasonic velocity and density of alpha silicon carbide. Data for material in as sintered and hot isostatically pressed conditions, and three grain sizes (Klima et al, 1981).

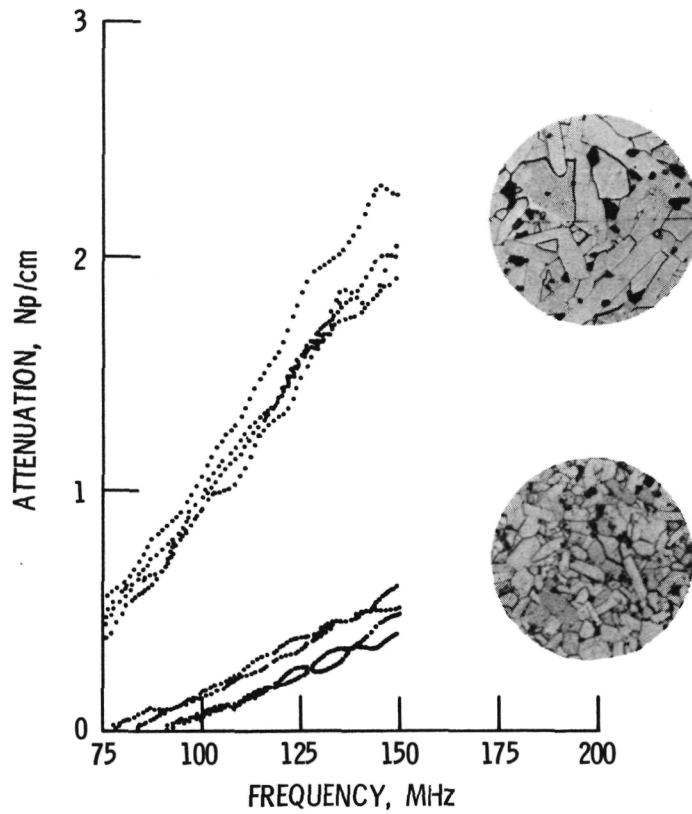


Figure 7. - Effect of microstructure on ultrasonic attenuation in sintered alpha silicon carbide. Bulk density, 3.11 to 3.12 g/cm³.

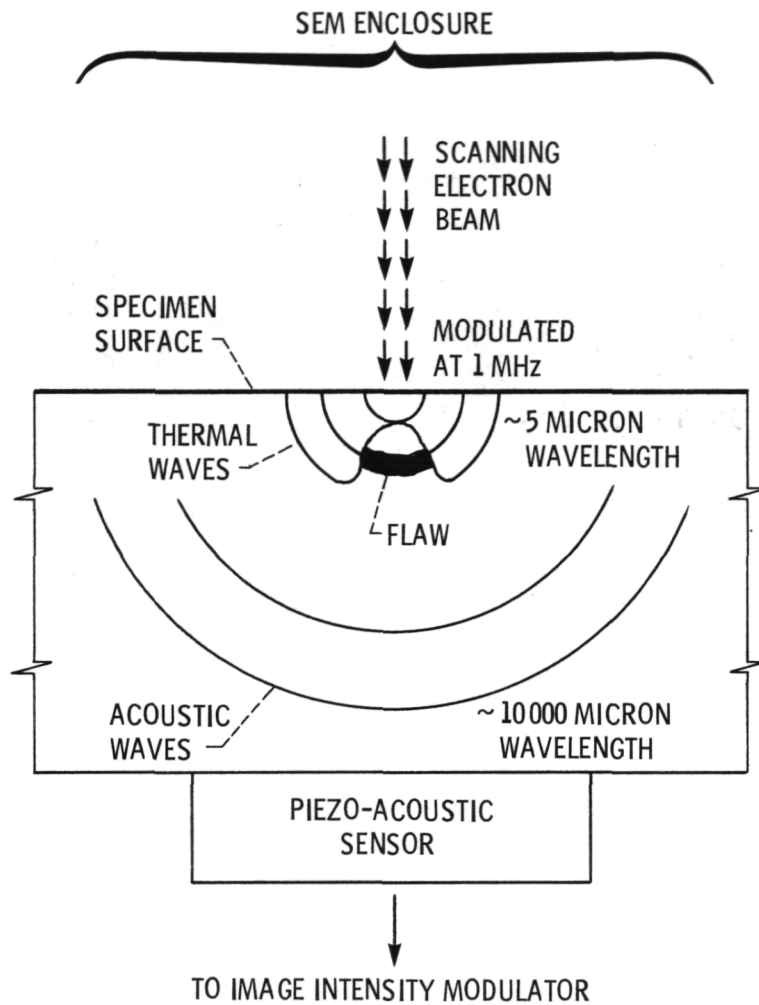
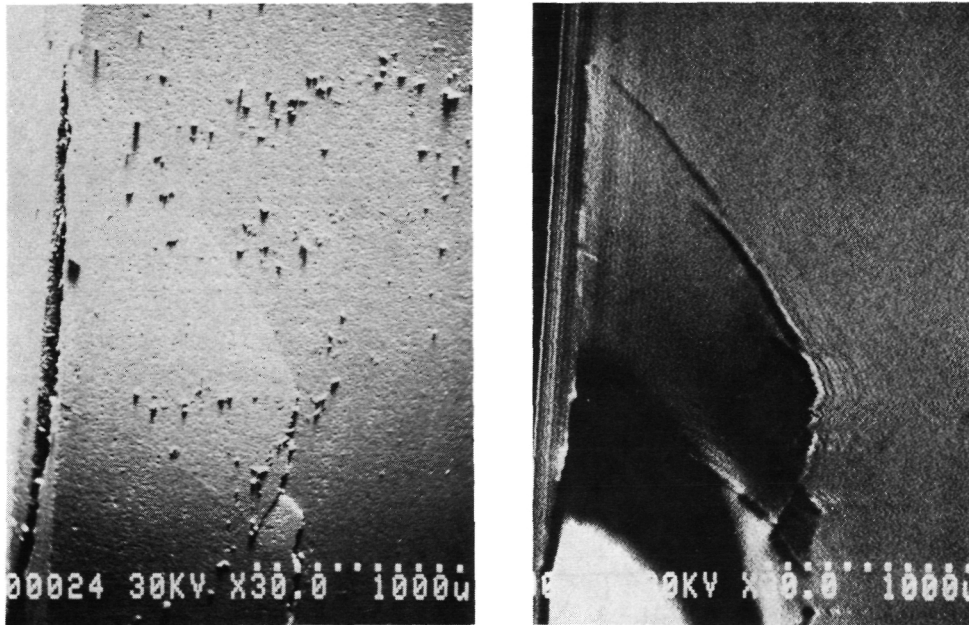


Figure 8. - Schematic representation of a thermo-acoustic device utilizing an electron beam source and an ultrasonic sensor housed in a scanning electron microscope enclosure.

ORIGINAL PAGE IS
OF POOR QUALITY



(a) SEM backscatter image.

(b) Thermo-acoustic image.

Figure 9. - Images of a spall crack near the edge of a silicon carbide MOR bar obtained by a conventional SEM technique and by thermo-acoustic microscopy (TAM). TAM reveals subsurface cracking not shown by SEM. Dust visible in the SEM image was ignored by TAM.

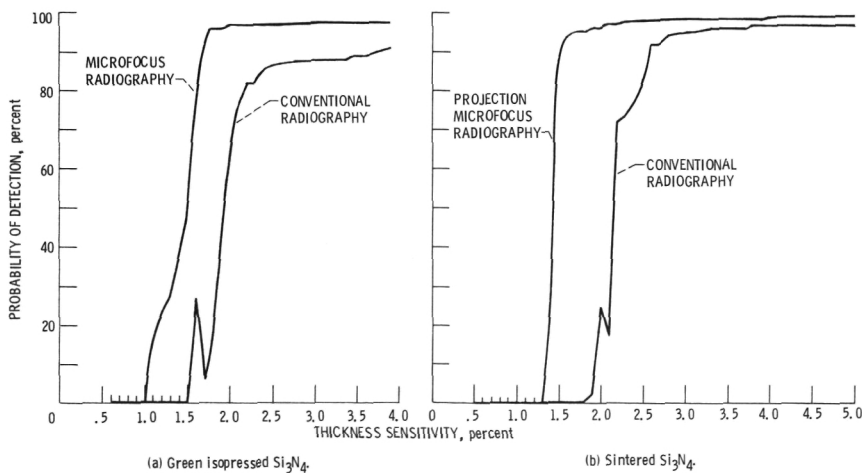


Figure 10. - Lower bound probability of detection of surface voids in Si_3N_4 bars calculated at 95 percent confidence level. Thickness sensitivity = (void dimension in x-ray beam direction)/(thickness of specimen in same direction). (Baakjini, et al)

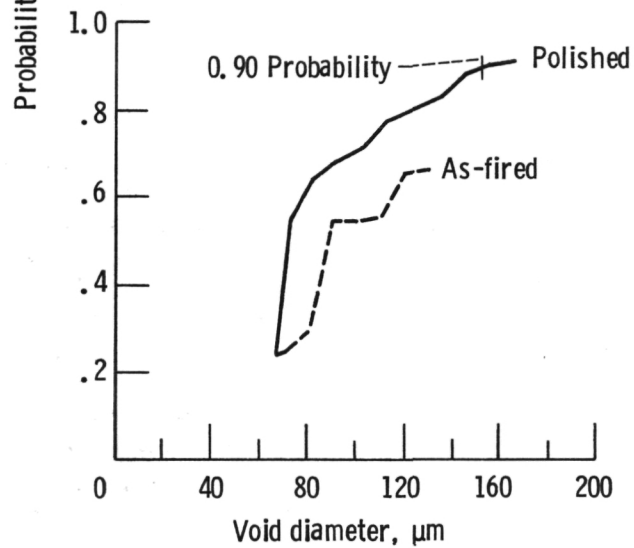
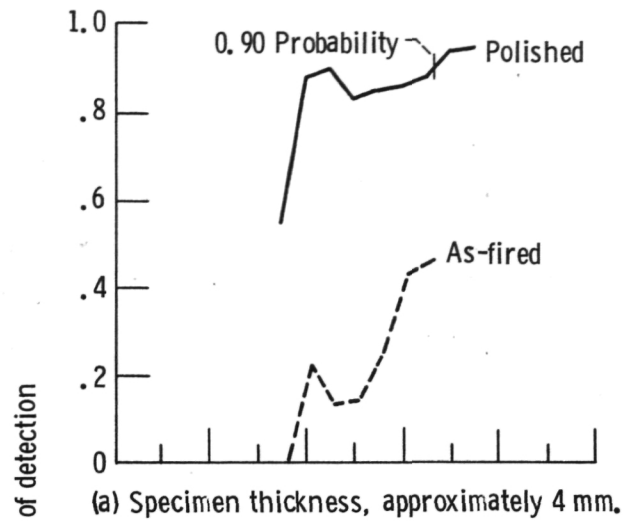


Figure 11. - Probability of detection of voids in sintered silicon nitride specimens showing improvement in void detectability after hand polishing. Probability of detection calculated at 0.95 confidence level. (Roth, et al)

1. Report No. NASA TM-87186		2. Government Accession No.		3. Recipient's Catalog No.	
4. Title and Subtitle NDE of Structural Ceramics				5. Report Date	
				6. Performing Organization Code 506-53-1A	
7. Author(s) Stanley J. Klima and Alex Vary				8. Performing Organization Report No. E-2840	
				10. Work Unit No.	
9. Performing Organization Name and Address National Aeronautics and Space Administration Lewis Research Center Cleveland, Ohio 44135				11. Contract or Grant No.	
				13. Type of Report and Period Covered Technical Memorandum	
12. Sponsoring Agency Name and Address National Aeronautics and Space Administration Washington, D.C. 20546				14. Sponsoring Agency Code	
15. Supplementary Notes Prepared for the 31st International Gas Turbine Conference, sponsored by the American Society of Mechanical Engineers, Dusseldorf, West Germany, June 8-12, 1986.					
16. Abstract Radiographic, ultrasonic, scanning laser acoustic microscopy (SLAM), and thermo-acoustic microscopy techniques were used to characterize silicon nitride and silicon carbide modulus-of-rupture test specimens in various stages of fabrication. Conventional and microfocus x-ray techniques were found capable of detecting minute high density inclusions in as-received powders, green compacts, and fully densified specimens. Significant density gradients in sintered bars were observed by radiography, ultrasonic velocity, and SLAM. Ultrasonic attenuation was found sensitive to microstructural variations due to grain and void morphology and distribution. SLAM was also capable of detecting voids, inclusions and cracks in finished test bars. Consideration is given to the potential for applying thermo-acoustic microscopy techniques to green and densified ceramics. The detection probability statistics and some limitations of radiography and SLAM also are discussed.					
17. Key Words (Suggested by Author(s)) Nondestructive evaluation; Nondestructive testing; Ultrasonics; Radiography; Photo-acoustic microscopy; Thermoacoustic microscopy; Ceramics; Materials characterization			18. Distribution Statement Unclassified - unlimited STAR Category 38		
19. Security Classif. (of this report) Unclassified		20. Security Classif. (of this page) Unclassified		21. No. of pages	22. Price*

National Aeronautics and
Space Administration

Lewis Research Center
Cleveland, Ohio 44135

Official Business
Penalty for Private Use \$300

SECOND CLASS MAIL

ADDRESS CORRECTION REQUESTED



Postage and Fees Paid
National Aeronautics and
Space Administration
NASA-451

NASA
